Article type: Original Paper

Title: Resonant transmission through topological metamaterial grating

Hongwei Jia[1,2], Wenlong Gao[2], Yuanjiang Xiang[1,], Haitao Liu[3] and Shuang Zhang[2,†]*

*Corresponding Author: E-mail: *xiangyuanjiang@126.com, †s.zhang@bham.ac.uk

[1]SZU-NUS Collaborative Innovation Center for Optoelectronic Science & Technology, Key Laboratory of Optoelectronic Devices and Systems of Ministry of Education and Guangdong Province, Collage of Optoelectronic Engineering, Shenzhen University, Shenzhen 518060, China.
[2]School of Physics & Astronomy, University of Birmingham, Birmingham B15 2TT, UK
[3]Key Laboratory of Optical Information Science and Technology, Ministry of Education, Institute of Modern Optics, Nankai University, Tianjin 300071, China.

Abstract: Recently, artificial photonic structures that exhibit nontrivial topological properties have attracted growing attention due to their capability of achieving one-way backscatter immune transport of light. While photonic crystals are predominantly employed for achieving nontrivial topologies, effective medium approach based on metamaterials has been recently proposed for realizing topologically protected unidirectional surface states. In this paper we construct a microscopic model to investigate the transmission of topological metamaterial grating based on the scattering processes involving unidirectional surface states. The numerically simulated transmission efficiency of the grating can be precisely reproduced by the model. Our model demonstrates that the sharp transmission resonance of the grating results from the constructive interference of the topologically protected one-way surface states. The present work provides an intuitive picture for understanding the scattering processes and resonance behaviors of the topologically protected one-way surface states. Benefitting from the sharp spectral features of the supported resonances, the proposed grating structure may be potentially used for sensing applications.

1. Introduction

Surface states, especially surface plasmon polaritons (SPPs) at the interface between a noble metal and a dielectric material, play an important role in the current development of nano-photonics. The resonant excitation of SPPs underlies various interesting phenomena, such as extraordinary optical transmission (EOT) [1-4], enhancements of spontaneous emission or electromagnetic field [5-9], and surface enhanced Raman spectroscopy (SERS) [10-12]. At the boundary of ordinary materials, the propagation of the surface states is highly dependent on the geometry of the material boundary and always suffers from energy loss at sharp steps due to back scattering. Driven by the recent development of topological physics [13-15], quantum systems with topological properties are proposed to achieve one-way transport of electrons at the surface or edge [16-21]. Different from ordinary materials, surface states supported by such systems are completely dependent on the bulk Hamiltonian, and the propagation of these states is robust against perturbations at the boundary of the material, such that these states are said to be topologically protected against disorder. This is called the bulk-edge correspondence. Because of this superior property, these surface states can be widely applicable to quantum information processing for overcoming energy dissipation.

The concept of nontrivial topology in solid state systems has been extended to photonic systems, with particular interests focusing on achieving one-way surface states in different optical systems such as photonic crystals, metamaterials and magnetized plasma [22-43]. Optical analogues of quantum Hall effect [23,24,28,31,34] and quantum spin Hall effect have been realized in various 2D photonic crystal systems [25,27,29]. Introducing time reversal symmetry breaking or spin orbit coupling to these systems results in nontrivial bandgaps, wherein gapless unidirectioanl surface states can appear [23-25,27-29,31,34]. In 3D photonic systems, there has been growing attention on Weyl degeneracies, 3D Dirac points, and weak photonic topological insulators [22,30,35,38,41-43]. The optical Weyl degeneracies can be obtained by introducing inversion symmetry breaking in photonic crystals or metamaterials

[22,35,41,43], or time reversal symmetry breaking in magnetized plasma [38]. The Weyl points are highly robust as they can only be eliminated when two Weyl points of opposite chiralities meet and annihilate each other. In particular, effective media approaches have been proposed for achieving Weyl deneracies in metamaterials [35,38]. It was theoretically demonstrated that one-way backscatter immune surface states, the so called Fermi arcs, can be supported at the interface between a chiral hyperbolic metamaterial and a topologically trivial medium [35]. This type of metamaterials were recently realized, leading to experimental observation of unidirectional surface states [41,43].

Previous studies on topological metamaterials have focused on systems with homogeneous effective electromagnetic properties. Thus far, there have been no exploration on composite photonic structures with topological metamaterials as the constituent materials, which may introduce new interesting topological phenomena. In this article, we propose a grating made of one type of topological metamaterial - chiral hyperbolic metamaterials. It is observed that when the in-plane wave vector lies within the nontrivial gap between the two equi-frequency surfaces of bulk modes where unidirectional surface states can be excited, the transmission efficiency of the grating displays sharp resonance peaks. To identify the role of unidirectional surface state on the transmission resonance, we build a model by considering the multiple scattering processes of the unidirectional surface states at the corners of the rectangular gratings. The transmission efficiency of the grating can be well reproduced with the model. By using the model, the geometrical parameters of the grating for achieving the resonance condition can be obtained. It is found that if the width or height of the metamaterial gratings is within the decay length of the surface state, the predicted transmission efficiency slightly deviates from the rigorous calculations, owing to the coupling of the surface states at adjacent interfaces. The present work provides an intuitive picture for understanding the

scattering processes and resonance behaviors of the one-way topological surface states, and may also provide a new prospective for the design of refractive index sensing devices.

2. Structure and Theoretical Model

The considered structure is schematically shown in Fig. 1(a). The yellow region represents the newly developed photonic Weyl semimetal [35,41,43], chiral hyperbolic metamaterial (CHM), whose electromagnetic property can be described with the constitutive equation $\mathbf{D}=\varepsilon_0\boldsymbol{\varepsilon}_r\mathbf{E}-i\gamma\mathbf{H}/c$, $\mathrm{B}=\mu_0\boldsymbol{\mu}_r\mathrm{H}+i\gamma\mathbf{E}/c$. In this equation, $\boldsymbol{\varepsilon}_r$ and $\boldsymbol{\mu}_r$ denote the relative dielectric permittivity and magnetic permeability tensors, and γ is the introduced chirality of the material. Other parameters, ε_0, μ_0 and c denote the dielectric constant, magnetic permeability and light speed in vacuum, respectively. The CHM features three topologically distinct bulk equi-frequency surfaces (EFSs) in the k space - two hyperbolic-like EFSs and a closed elliptical one in the middle. Unidirectional surface states exist within the gaps between the three bulk EFSs [35] due to the nonzero Chern number on each EFS. Here we use the design in Ref. 35 by setting $\boldsymbol{\varepsilon}_r=\mathrm{diag}(4,-3,4)$, $\boldsymbol{\mu}_r=0.5$ and $\gamma=0.5$. While this is an idealized chiral hyperbolic metamaterial, it may provide a platform for designing practical structures as experimentally realized in [41,43]. The width and height of the metamaterial are denoted as L and h, and two adjacent metamaterial cylinders are separated by an air gap (refractive index being 1) with width $w=0.3\lambda$. The upper and lower substrates shaded in blue are made from a high refractive-index media (refractive index $n_h=3$), and the gap between the substrate and the grating layer is $d=0.2\lambda$, such that light incident from high index region can couple evanescently with the surface mode supported by the metamaterial grating. The grating is illuminated by a TM (magnetic field vector x-polarized) polarized plane wave from the lower substrate, with the plane of incidence perpendicular to x axis and the incidence angle being θ.

We plot the EFSs of the chiral hyperbolic metamaterial. It is shown that the unidirectional surface state lies in the gap regions $0.97k_0<k_y<1.90k_0$ and $-1.90k_0<k_y<-0.97k_0$

(with $k_0=2\pi/\lambda$, $k_y=n_h k_0 \sin\theta$ and λ being the wavelength) since the Chern numbers on different EFSs are nonzero [in Fig. 1(b)]. To theoretically investigate the contribution of the unidirectional surface states to the transmission of the grating, in the following calculations we set the in-plane wave vector of the incident plane wave $k_y=1.5k_0$, so that surface states can be efficiently excited. Under this condition, the surface state is expected to propagate in a helical trajectory as schematically shown in Fig. 1(c). Next we will derive an analytical expression of the transmission efficiency based on the multiple scattering processes of the unidirectional surface states. The unidirectional surface state at the metamaterial boundary is exactly the fundamental propagative waveguide mode [44], whose propagation constant and field distribution can be easily derived via numerical tools by treating the metamaterial boundary as a waveguide.

The numerical results throughout this article are obtained with the rigorous coupled wave analysis (RCWA) [45,46] that are often used in modelling periodic electromagnetic systems. RCWA can also be used to model non-periodic systems by employing perfectly matched layers, which is called the aperiodic Fourier modal method (a-FMM) [47,48]. We first obtain the field distributions of the surface states at the boundaries of metamaterial cylinders. In the air gap between adjacent metamaterials cylinders [indicated by Region E in Fig. 1(a)], there exist two counter-propagating surface states, which are shown in Figs. 2(a)-2(b). It is seen that the downward surface state is bounded to the left boundary, whereas the upward surface state is bounded to the right boundary. However, at the upper and lower boundaries of the metamaterial cylinder [region F and G in Fig. 1(a) respectively] the unidirectional surface states are leaky modes due to the presence of high refractive index of the substrates. Figures 2(c)-2(d) show the field distribution of the leaky states at the upper and lower boundaries of the metamaterial cylinder respectively. It is seen that energy leakage exists at the upper [Fig. 3(c)] and lower [Fig. 3(d)] layers as the field is radiating away from the interface between

metamaterial and high index media, as a result of which, the surface states intensity attenuates gradually along the propagation direction. It is shown that the surface states penetrate into the metamaterial, so that for a grating with small width or height of the metamaterial cylinder (L or h), the surface states couple across the metamaterial to the opposite boundaries. To simplify the modelling, we neglect this coupling effect, whose impact on the grating transmission can be tested with the comparison between the rigorous numerical results and model predictions.

With the illumination of incident plane wave from the lower substrate, the bounded and leaky surface states on the boundaries can be excited. Here we use A, B, C and D to denote the complex amplitude coefficients of the surface states [see Fig. 3(a)]. For simplicity, we only consider the co-polarization transmission efficiency with the incident plane waves being TM polarized (magnetic field vector x-polarized). For other cases [TM to TE (electric field vector x-polarized), TE to TE and TE to TM], the transmission efficiency is much smaller as detailed in Fig. S1 in the Supporting Information. By considering the excitation and scattering processes of these surface states, the complex amplitude coefficients satisfy a set of coupled mode equations,

$$A = \beta + Bu\rho + Du'\alpha, \tag{1a}$$

$$C = Au\alpha' + Cu'\tau, \tag{1b}$$

$$B = Au\rho + Cu'\alpha, \tag{1c}$$

$$D = \kappa + Bu\alpha' + Du'\tau, \tag{1d}$$

where u=exp($ik_0 n_{\mathrm{eff,B}} h$) and u'=exp($ik_0 n_{\mathrm{eff,L}} L$) denote the phase shifts of the bounded and leaky surface states across the corresponding side of the rectangular cylinder, with $n_{\mathrm{eff,B}}$ and $n_{\mathrm{eff,L}}$ being the complex effective index of the bounded and leaky surface states that can be obtained with aperiodic Fourier Modal Method (a-FMM) [47,48]. β and κ [see Fig. 3(b)] denote the excitation coefficients of bounded and leaky surface states under the illumination

of a TM polarized plane wave. The scattering coefficient from bounded to leaky surface states is denoted by α' [see Fig. 3(e)], and the reciprocal coefficient is denoted by α [see Fig. 3(f)]. At the upper or lower substrate, the bounded surface state is partially reflected back, with the reflection coefficient represented by ρ [see Fig. 3(e)]. Similarly, we use τ to denote the transmission coefficient of the leaky surface state across the air gap between metamaterial cylinders [see Fig. 3(e)]. All these scattering coefficients (β, κ, α, α', ρ and τ) can be rigorously calculated with the a-FMM incorporating the mode orthogonality theorem [44,49] (Supporting Information provides the derivation details of the equation of mode orthogonality theorem for bi-anisotropic media waveguide). Equation (1) can be understood intuitively. For example, the first equation of Eq. (1) shows that the upward bounded surface wave results from three contributions: a direct excitation from the incident TM plane wave with excitation coefficient β; the reflection (ρ) of the down-going bounded state with an amplitude B and a phase u; the scattering (α) of the left-going leaky surface state with an amplitude D and a phase u'. The other equations can be understood in a similar manner. Once the amplitude coefficients of surface states are obtained, the zero-order transmission coefficient of the TM plane wave t_A [Fig. 3(a)] can be expressed as,

$$t_A = (Au\beta' + Cu'\kappa')\lambda / \Lambda, \tag{2}$$

where $\Lambda=L+w$ denotes the period of the grating. Intuitively, Equation (2) shows that the transmitted plane wave results from the scattering [with scattering coefficient β' defined in Fig. 3(c)] of the upward bounded state (with amplitude A and a phase shift u) and the scattering [with scattering coefficient κ' in Fig. 3(d)] of the right-going leaky state (with amplitude B and a phase shift u'). The coefficients β' and κ' are reciprocal coefficients of β and κ, and can be calculated with the reciprocity relation [44]. Solving Eqs. (1)-(2), the transmission coefficient t_A of TM plane wave can be obtained analytically,

$$t_A = \frac{u(\beta + \frac{\kappa u'\alpha}{1-u'\tau})(\beta' + \frac{\alpha' u'\kappa'}{1-u'\tau})}{1-u^2(\rho + \frac{\alpha' u'\alpha}{1-u'\tau})^2}\lambda/\Lambda, \quad (3)$$

and thus the transmission efficiency of the zero-order diffraction wave is given by $T_0=|t_A|^2$.

2. Impact of geometrical parameters on the transmission of the grating

In this section, we will discuss the impact of two important geometrical parameters, the height h and width L of the metamaterial cylinder, on the transmission of the metamaterial grating, and provide a physical insight of the transmission resonance with the theoretical model.

2.1. Impact of Cylinder Height on the Transmission Efficiency

We first calculate the transmission efficiency of the zero-order diffraction wave with the rigorous couple wave analysis (RCWA). The results are plotted as a function of the height h in Fig. 4 for different widths of the metamaterial grating. It is seen that the transmission efficiency T_0 oscillates periodically as the height h varies. For comparison, we also calculate the transmission efficiency using Eq. (3) of the model, with the results shown as the blue solid curves in Fig. 4. The model nicely reproduces the resonance behaviors of the transmission efficiency. However, for very small width L or height h of the metamaterial cylinders, the predicted results of the model start to deviate from the rigorous RCWA data, which is due to the coupling effect of the surface states that is neglected in the model. Based on Eq. (3), the transmission efficiency can be maximized under a phase-matching condition,

$$2[k_0 n_{\text{eff,B}} h + \arg(\rho + \frac{\alpha' u'\alpha}{1-u'\tau})] = 2m\pi, \quad (4)$$

where m is a negative integer (because the complex effective indices are negative, as detailed in the caption of Fig. 2) corresponding to different resonance orders. For the case that the in-plane wave vector being $k_y=1.5k_0$, the scattering coefficients are $\alpha=0.67+0.75i$ and $\alpha'=0.66+0.76i$, with $\arg(\alpha)=48°$and $\arg(\alpha')=49°$ respectively, which means that surface states experience a phase shift across the corner. The product $\alpha' u' \alpha$ denotes the phase shift and

damping of the bounded surface state across an upper or lower boundary of the metamaterial cylinder, which is slightly less than unity due to the energy conservation relation [50]. The lossless case with $|u|=1$ yields $\left|u^2(\rho+\frac{\alpha' u' \alpha}{1-u'\tau})^2\right| \approx 1$, so that the denominator in Eq. (3) can be minimized under the phase-matching condition of Eq. (4). The phase-matching condition Eq. (4) can be further simplified by considering the following approximations. Since the backward reflection of bounded surface state at the substrate and the transmission of leaky surface state across the air gap are quite weak due to topological protection, $|\rho|$ and $|\tau|$ are nearly zero. On the other hand, the other coefficients $|\alpha'|$, $|u'|$ and $|\alpha|$ are very close to 1 because of the very small amount of energy leakage. By approximating the coefficients ρ and τ to be zero, we obtain a simplified version of phase-matching condition,

$$2[k_0 n_{\text{eff,B}} h + k_0 \,\text{Re}(n_{\text{eff,L}})L + \arg(\alpha') + \arg(\alpha)] = 2m\pi, \quad (5)$$

The resonance peaks predicted with Eq. (5) agree well with the rigorous numerical results, as shown by Fig. 4. Equation (5) provides an intuitive picture that at resonances, the phase shift of the surface states across all four boundaries of the metamaterial cylinder is multiples of 2π, resulting in a constructive interference of the surface states. Thus the model provides an intuitive understanding of the resonance behavior of the transmission efficiency of the metamaterial grating.

2.2. Impact of Cylinder Width on the Transmission Efficiency

Another important geometrical parameter that determines the resonance of the grating transmission is the width of the metamaterial cylinder L. To investigate this in detail, here we calculate the transmission efficiency as a function of L with RCWA, and results are shown in Fig. 5(a). Note that the height is set to be a large value $h=2.0\lambda$, and the width L ranges from 0.5λ to 4.0λ in this calculation, so that the coupling effect of the leaky and the bounded surface states is negligible, hence ensuring the accuracy of the model predictions. Figure 5(a)

shows that the transmission efficiency also oscillates periodically as the width L varies. Interestingly, different from the plots in Fig. 4, the transmission efficiency reaches the minimum values (which is called valley hereafter) when the order of resonance m is even, and the peak value of transmission efficiency is attenuating with the increase of the resonance order $|m|$. To show the underlying physics, we calculate the transmission efficiency with the model of Eq. (3), and results are plotted with the blue solid curve in Fig. 5(b). Very good agreement can be seen in this figure. Since the coefficients ρ and τ are negligible compared with other quantities, the expression of transmission t_A in Eq. (3) can be approximated in the form

$$t_A = \frac{u(\beta + \kappa u'\alpha)(\beta' + \alpha' u'\kappa')}{1 - u^2(\alpha' u'\alpha)^2}\,\lambda / \Lambda. \tag{6}$$

It is shown that the numerator is actually a product of two interferences: the first interference S1=$\beta+\kappa u'\alpha$ is between the two surface states launched by the incident plane wave at the two lower corners, and the second interference S2=$\beta'+\alpha' u'\kappa'$ is between the two out-going plane waves due to the scattering of surface states at the two upper corners. Both S1 and S2 are maximized (constructive interference) or minimized (destructive interference) simultaneously with the oscillation period determined by the phase factor u', as numerically shown in Fig. 5(b) with black-solid and red-dashed curves. Note that β, κ and α are proportional to β', κ' and α' due to reciprocity, respectively. Different from S1 and S2, the oscillation period of the denominator S3=$1-u^2(\alpha' u'\alpha)^2$ in Eq. (6) are determined by u^2, which means that the oscillation period of S3 is half of that of S1 or S2, just as shown with the blue curve in Fig. 5(b). Accidentally, for the case of $h=2.0\lambda$, S1 and S2 are minimized at the odd resonances predicted by the phase matching condition, which leads to presence of the valley of the transmission efficiency. For other cases, the valley values are present at the same position, but mostly are not at the resonances, as numerically shown in Supporting Information Fig. S2. Thus we can conclude that the presence of valley values of the transmission efficiency in Fig.

4 is determined by the destructive interference of the launched surface states by incident plane wave at the lower corners and that of the out-going plane wave scattered by surface states at the upper corners.

3. Topological Metamaterial Grating Used for Refractive Index Sensing

The topological metamaterial grating has a great potential in achieving high resolution in the refractive index sensing. If one fills a liquid with refractive index n_a into the gaps in the grating [see Fig. 1(a), the complex effective indices of the bounded and leaky surface states ($n_{\text{eff,B}}$ and $n_{\text{eff,L}}$) will change as n_a and k_y vary. According to the phase matching condition in Eq. (5), the position of the resonance peaks can be very sensitive to the values of n_a and k_y. In Fig. (6), we plot the transmission efficiency as functions of the index n_a, and the sharp resonance peaks can be observed as n_a varies. The resolution of the refractive index sensing is determined by the slope $\Delta T_0 / \Delta k_y$, such that in the vicinity of the resonance peaks, the resolution can be extremely high. Besides, the position of the peak can be easily tuned by the in plane wave vector k_y, as shown by the comparison between the red, black and blue solid curves in Fig. (6). The above results indicate that by selecting an appropriate angle of incidence θ (so as to tune k_y) according to the approximate value of n_a, the accurate value of na can thus be easily derived by measuring the transmission efficiency T_0. As a conclusion, the topological metamaterial grating provides a new platform for the sensing of refractive index with high resolutions.

Conclusion

In this article, we have investigated the transmission of light through a grating made of chiral hyperbolic metamaterials. To investigate the effect of topologically protected unidirectional surface state on the resonant transmission of the grating, we build a microscopic model by considering the multiple scattering processes of the surface state, and the coupling effect with the adjacent metamaterial boundaries of the surface state is neglected for simplicity. The

model can nicely reproduce the transmission efficiency as a function of geometrical parameters of the rectangular metamaterial cylinder. Deviation can be found for the cylinder with very small values of height or width, which is attributed to the impact of the coupling effect that is neglected within the model. Interestingly, the transmission efficiency exhibits alternative peak and valley values of transmission efficiency as the cylinder width varies. The present work clearly illustrates the scattering and resonance behaviors of the unidirectional surface states on the topological metamaterial boundaries, and the role of the surface states on the transmission of the metamaterial grating is well identified. Similar scattering processes might be useful for understanding the scattering behaviors of the one-way surface Bloch waves that are supported by topological photonic crystals [24,25]. The proposed grating structure also has a great potential in the refractive index sensing with high resolutions.

Supporting Information

Additional supporting information may be found in the online version of this article at the publisher's website.

Acknowledgements

This project is partially supported by National Science Foundation of China (Grant No. 61490713). S. Z. acknowledges the support from ERC Consolidator Grant (TOPOLOGICAL), Horizon 2020 Action Project No. 734578 (D-SPA), the Engineering and Physical Sciences Research Council (EP/J018473/1), and the Royal Society Wolfson Research Merit Award.

Received: ((will be filled in by the editorial staff))
Revised: ((will be filled in by the editorial staff))
Published online: ((will be filled in by the editorial staff))

Keywords: Topological photonics; Metamaterials; Grating; Unidirectional surface states; transmission resonance

References

[1] T. W. Ebbesen, H. J. Lezec, H. F. Ghaemi, T. Thio, P. A. Wolff, *Nature* **391**, 667-669 (1998).

[2] J. A. Porto, F. J. Garcia-Vidal, J. B. Pendry, *Phys. Rev. Lett.* **83**, 2845 (1999).

[3] L. Martin-Moreno, F. J. Garcia-Vidal, H. J. Lezec, K. M. Pellerin, T. Thio, J. B. Pendry, T. W. Ebbesen, *Phys. Rev. Lett.* **86**, 1114 (2001).

[4] H. Liu, P. Lalanne, *Nature*, **452**, 728-731 (2008).

[5] S. Eustis, M. A. El-Sayed, *Chem. Soc. Rev.* **35**, 209-217 (2006).

[6] J. N. Anker, W. P. Hall, O. Lyandres, N. C. Shah, J. Zhao, R. P. Van Duyne, *Nat. Materials* **7**, 442-453 (2008).

[7] S. Kühn, U. Håkanson, L. Rogobete, V. Sandoghdar, *Phys. Rev. Lett.* **97**, 017402 (2006).

[8] C. Sauvan, J. P. Hugonin, I. S. Maksymov, P. Lalanne, *Phys. Rev. Lett.* **110**, 237401 (2013).

[9] R. Esteban, G. Aguirregabiria, A. G. Borisov, Y. M. Wang, P. Nordlander, G. W. Bryant, J. Aizpurua, *ACS Photonics* **2**, 295-305 (2015).

[10] F. J. García-Vidal, J. B. Pendry, *Phys. Rev. Lett.* **77**, 1163 (1996).

[11] Y. Shen, X. Chen, Z. Dou, N. P. Johnson, Z. K. Zhou, X. Wang, C. Jin, *Nanoscale* **4**, 5576-5580 (2012).

[12] L. Li, S. Fang Lim, A. A. Puretzky, R. Riehn, H. D. Hallen, *Appl. Phys. Lett.* **101**, 113116 (2012).

[13] D. Xiao, M. C. Chang, Q. Niu, *Rev. Mod. Phys.* **82**, 1959 (2010).

[14] M. Z. Hasan, C. L. Kane, *Rev. Mod. Phys.* **82**, 3045 (2010).

[15] M. V.Berry, *Proc. R. Soc. London A* **392**, 45-57 (1984).

[16] X. L. Qi, S. C. Zhang, *Phys. Today* **1**, 63 (2010).

[17] X. L. Qi, S. C. Zhang, *Rev. Mod. Phys.* **83**, 1057 (2011)

[18] B. A. Bernevig, T. L. Hughes, S. C. Zhang, *Science* **314**, 1757-1761 (2006).

[19] C. L. Kane, E. J. Mele, *Phys. Rev. Lett.* **95**, 226801 (2005).

[20] C. Wu, B. A. Bernevig, S. C. Zhang, *Phys. Rev. Lett.* **96**, 106401 (2006)

[21] H. Xiong, J. A. Sobota, S. L. Yang, H. Soifer, A. Gauthier, M. H. Lu, Y. Y. Lv, S. H. Yao, D. Lu, M. Hashimoto, P. S. Kirchmann, Y. F. Chen, Z. X. Shen, *Phys. Rev. B* **95**, 195119 (2017).

[22] L. Lu, J. D. Joannopoulos, M. Soljačić, Topological photonics. *Nat. Photonics* **8**, 821-829 (2014).

[23] Z. Wang, Y. Chong, J. D. Joannopoulos, M. Soljačić, *Nature* **461**, 772-775 (2009).

[24] M. C. Rechtsman, J. M. Zeuner, Y. Plotnik, Y. Lumer, D. Podolsky, F. Dreisow, S. Nolte, M. Segev, A. Szameit, *Nature* **496**, 196-200 (2013).

[25] A. B. Khanikaev, S. H. Mousavi, W. K. Tse, M. Kargarian, A. H. MacDonald, G. Shvets, *Nat. Materials* **12**, 233-239 (2013).

[26] K. Fang, Z. Yu, S. Fan, *Nat. Photonics* **6**, 782-787 (2012).

[27] M. Hafezi, S. Mittal, J. Fan, A. Migdall, J. M. Taylor, *Nat. Photonics* **7**, 1001-1005 (2013).

[28] A. R. Davoyan, N. Engheta, *Phys. Rev. Lett.* **111**, 257401 (2013).

[29] C. He, X. C. Sun, X. P. Liu, M. H. Lu, Y. Chen, L. Feng, Y. F. Chen, *Proc. Natl. Acad. Sci.* **113**, 4924-4928 (2016).

[30] A. Slobozhanyuk, S. H. Mousavi, X. Ni, D. Smirnova, Y. S. Kivshar, A. B. Khanikaev, *Nat. Photonics* **11**, 130-136 (2017).

[31] W. Y. He, C. T. Chan, *Sci. Rep.* **5**, 8186 (2015).

[32] W. J. Chen, Z. Q. Zhang, J. W. Dong, C. T. Chan, *Nat. Commun.* **6**, 8183 (2015).

[33] A. Kumar, A. Nemilentsau, K. H. Fung, G. Hanson, N. X. Fang, T. Low, *Phys. Rev. B* **93**, 041413 (2016).

[34] D. A. Jacobs, A. E. Miroshnichenko, Y. S. Kivshar, A. B. Khanikaev, *New J. Phys.* **17**, 125015 (2015).

[35] W. Gao, M. Lawrence, B. Yang, F. Liu, F. Fang, B. Béri, J. Li, S. Zhang, *Phys. Rev. Lett.* **114**, 037402 (2015).

[36] M. G. Silveirinha, *Phys. Rev. B* **92**, 125153 (2015).

[37] M. Xiao, Q. Lin, and S. Fan, *Phys. Rev. Lett.* 117, 057401 (2016).

[38] W. Gao, B. Yang, M. Lawrence, F. Fang, B. Béri, S. Zhang, *Nat. Commun.* 7, 12435 (2016).

[39] S. A. H. Gangaraj, A. Nemilentsau, G. W. Hanson, *Sci. Rep.* **6** 30055 (2016).

[40] S. A. Skirlo, L. Lu, M. Soljačić, *Phys. Rev. Lett.* **113**, 113904 (2014).

[41] B. Yang, Q. Guo, B. Tremain, R. Liu, L. E. Barr, Q. Yan, W. Gao, H. Liu, Y. Xiang, J. Chen, C. Fang, A. Hibbins, L. Lu, S. Zhang. *Science* 2018: eaaq1221.

[42] Q. Guo, B. Yang, L. Xia, W. Gao, H. Liu, J. Chen, Y. Xiang, S. Zhang. *Phys. Rev. Lett.* **119**, 213901 (2017).

[43] B. Yang, Q. Guo, B. Tremain, L. E. Barr, W. Gao, H. Liu, B. Béri, Y. Xiang, D. Fan, A. P. Hibbins, S. Zhang. *Nat. Commun.* **8**, 97 (2017).

[44] A. W. Snyder, J. Love, *Optical waveguide theory* (Springer, New York, NY, USA, 2012).

[45] M. G. Moharam, T. K. Gaylord, E. B. Grann, D. A. Pommet, *J. Opt. Soc. Am. A* **12**, 1068-1076 (1995).

[46] L. Li, J. Opt. *J. Opt. A-Pure Appl. Opt.* **5**, 345 (2003).

[47] J. P. Hugonin, P. Lalanne, *J. Opt. Soc. Am. A* **22**, 1844-1849 (2005).

[48] The calculation is performed with an in-house software, Liu, H. T. *DIF CODE* for modeling light diffraction in nanostructures (Nankai University, Tianjin, China, 2010).

[49] H. Jia, Y. Xie, H. Liu, Y. Zhong, *J. Opt.* **18**, 055003 (2016).

[50] H. Liu, *Opt. Express* **21**, 24093-24098 (2013).

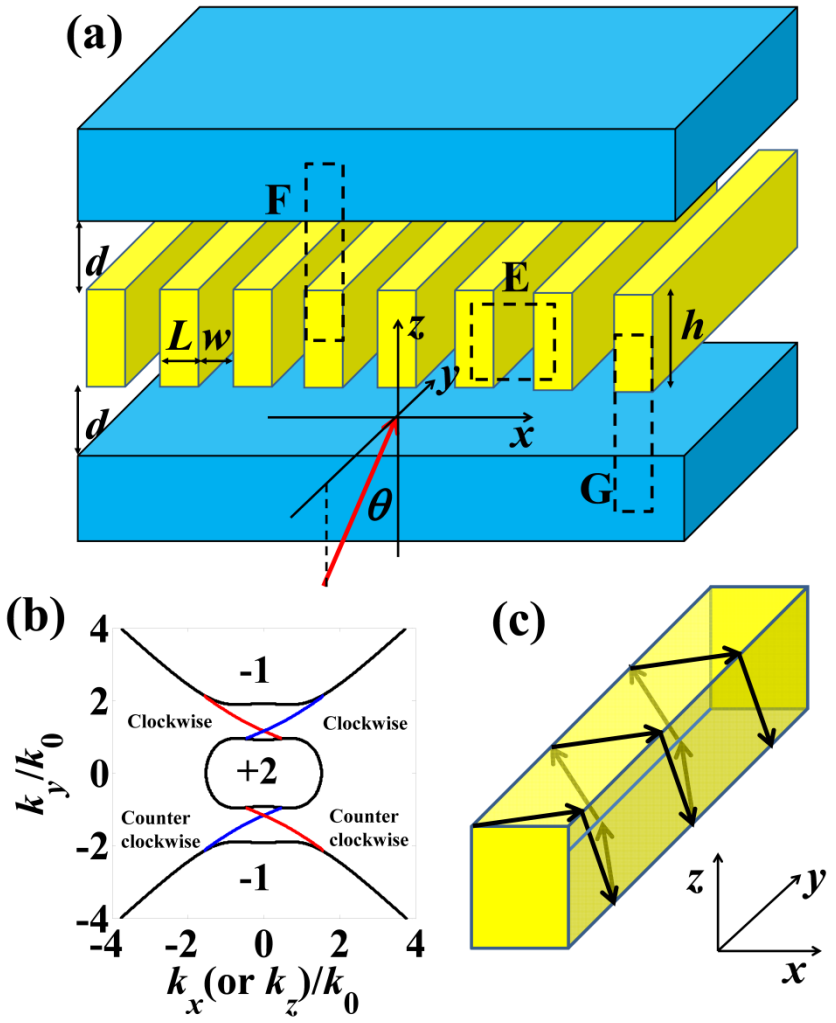

Figure 1. (a) Sketch of the grating. The yellow shade region denotes the chiral hyperbolic metamaterial, and the blue shaded region represents the high refractive index medium with refractive index n_h=3. The structure is illuminated by a TM polarized plane wave with the plane of incidence parallel to y-z plane and the incidence angle being θ. The squares E, F and G are in the plane of y=0. (b) Equi-frequency surfaces (EFSs) of the topological metamaterial, with the bulk states represented by black curves and surface states represented by red or blue curves, and +2, -1 representing the Chern numbers (see Ref. 35). The red curves denote the dispersion of the surface states on the upper and right surfaces in (c) and blue curves are for the lower and left surfaces in (c). The surface states are propagative clockwise and counter clockwise in the upper (k_y>0) and lower (k_y<0) EFSs gaps, respectively. (c) Propagating trace of the surface state on the interfaces of one metamaterial cylinder of the grating.

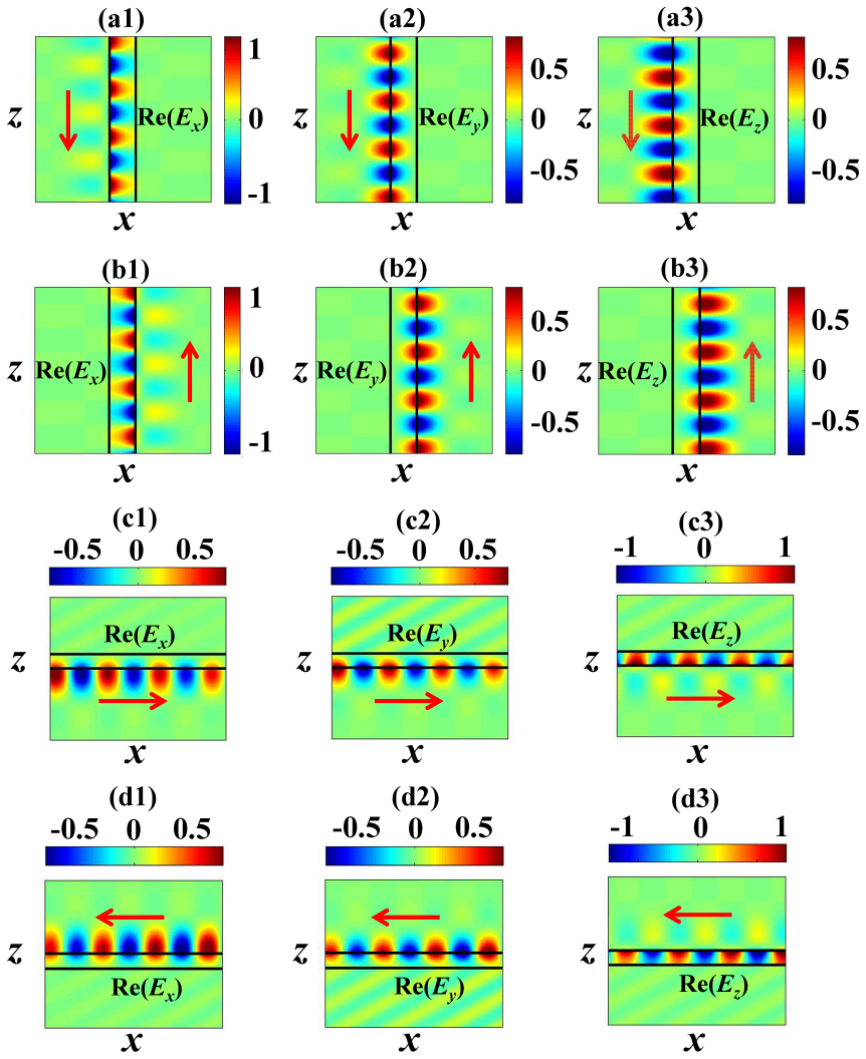

Figure 2. Distributions of the electric field of different surface states in plane y=0. (a)-(b) are for the downward and upward bounded surface states for the configuration surrounded by the square E in Fig. 1(a), the complex effective index $n_{\mathrm{eff,B}}$=–0.6500. (c)-(d) are for the right-going and left-going leaky surface states for the configurations surrounded by the squares F and G in Fig. 1(a) respectively, the complex effective index $n_{\mathrm{eff,L}}$=–0.6360+0.0125i. *The red arrows denote the propagation direction, and the left, middle and right columns represent the* E_x, E_y *and* E_z *components, respectively.* The results are obtained for k_y=1.5k_0.

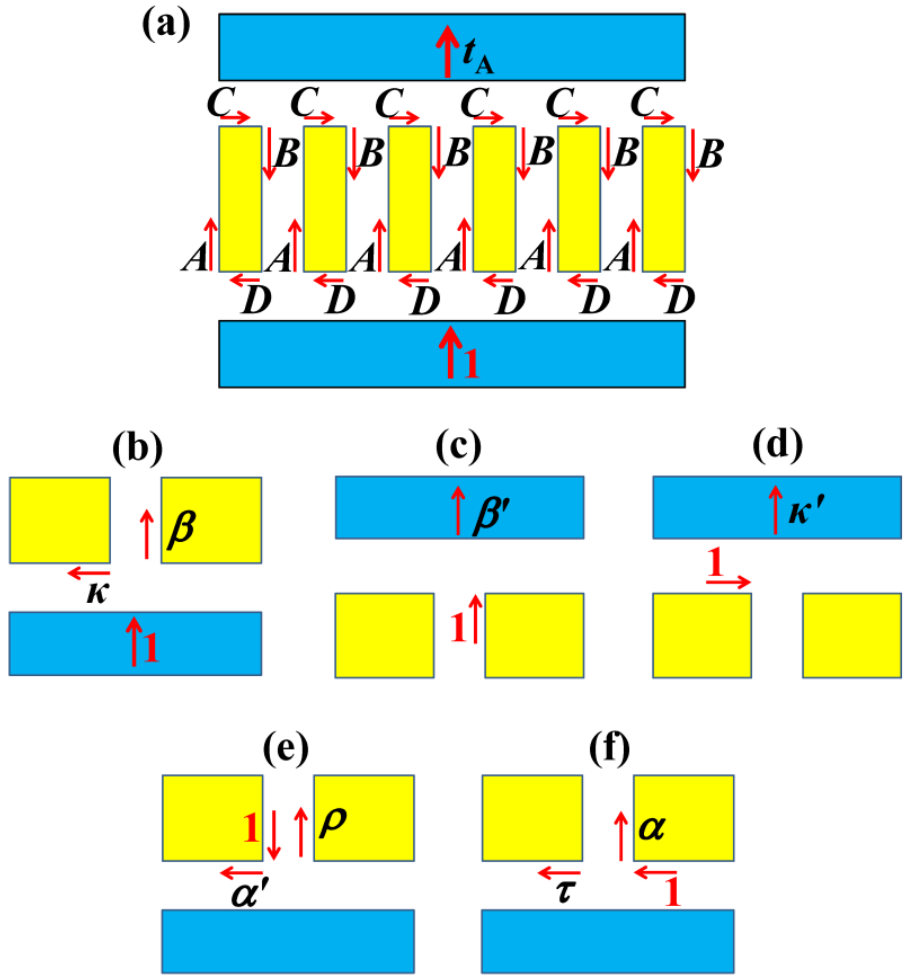

Figure 3. Physical quantities in building up the theoretical model. (a) Definition of the amplitude coefficients of surface states. *A* and *B* denotes the complex amplitude coefficients of the up-going and down-going bounded states with in the air gap, and *C* and *D* are defined similarly for the right-going and left-going leaky surface states. t_A denotes the transmission coefficient of the TM plane wave. (b)-(f) Definition of scattering coefficients that are used in the theoretical model [appeared in Eqs. (1)-(2)].

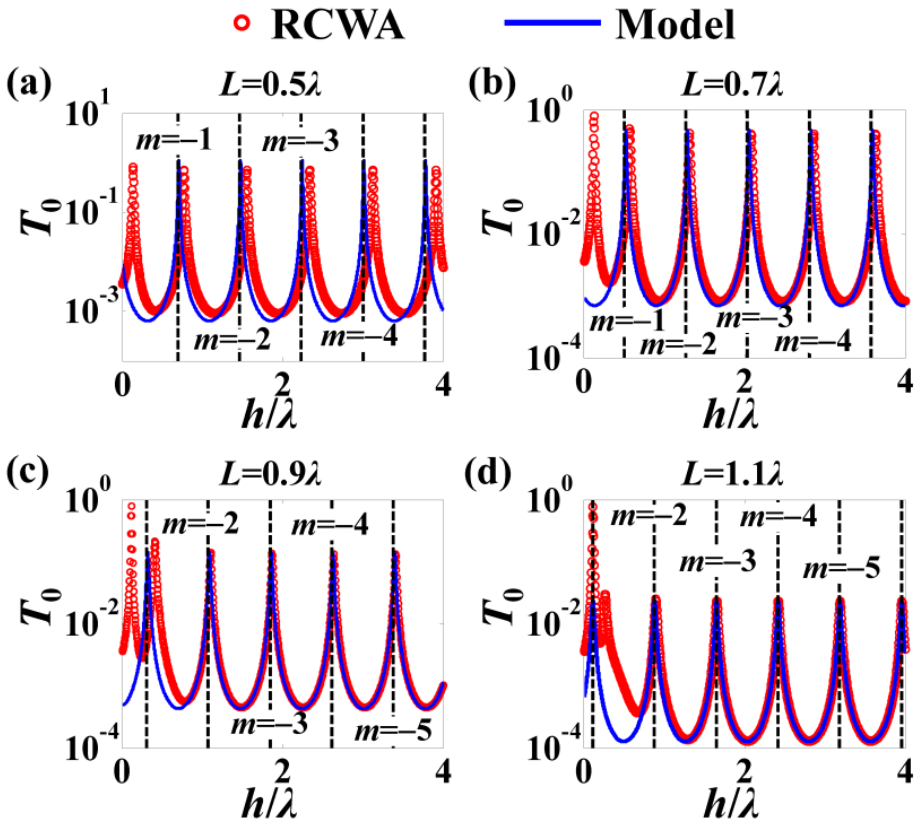

Figure 4. Zero-order transmission efficiency (T_0) plotted as a function of the height h of the metamaterial cylinder calculated with the RCWA (red circles) and the theoretical model (blue curves). (a)-(d) correspond to the width of the cylinder being L=0.5λ, 0.7λ, 0.9λ and 1.1λ, respectively. The vertical dashed lines denote different resonance orders that are calculated with the phase-matching condition [Eq. (5)].

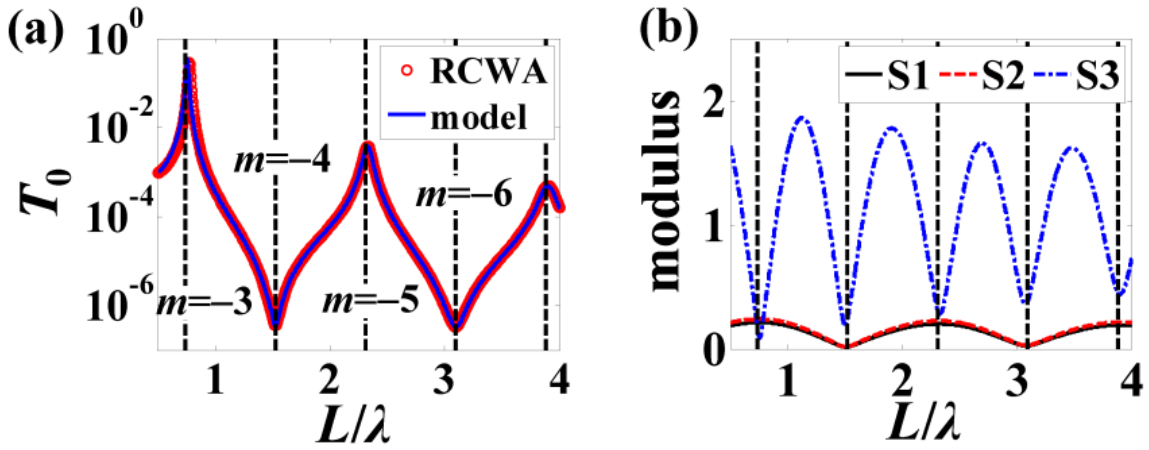

Figure 5. (a) Zero-order transmission efficiency (T_0) plotted as a function of the width L of the metamaterial cylinder calculated with the RCWA (red circles) and the theoretical model (blue curves). The negative integer m represents different resonance orders that are obtained with Eq. (5). (b) Moduli of the S1, S2 and S3 plotted as functions the width of the metamaterial L. The calculations are performed with the height of the cylinder being h=2.0λ.

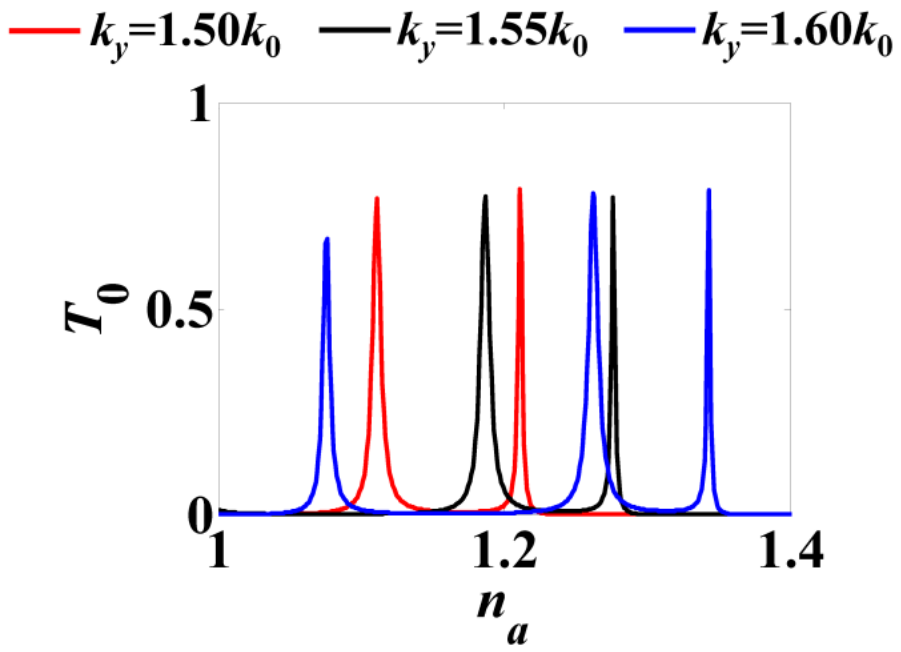

Figure 6. Topological metamaterial grating used for refractive index sensing. The red, black and blue solid curves represent the transmission efficiency T_0 as functions the index n_a of liquid filled in the gaps for the in plane wave vector k_y=1.50k_0, k_y=1.55k_0 and k_y=1.60k_0, respectively.

Supporting Information

Title: Resonant transmission through topological metamaterial grating

Hongwei Jia[1,2], Wenlong Gao[2], Yuanjiang Xiang[1,], Haitao Liu[3] and Shuang Zhang[2,†]*

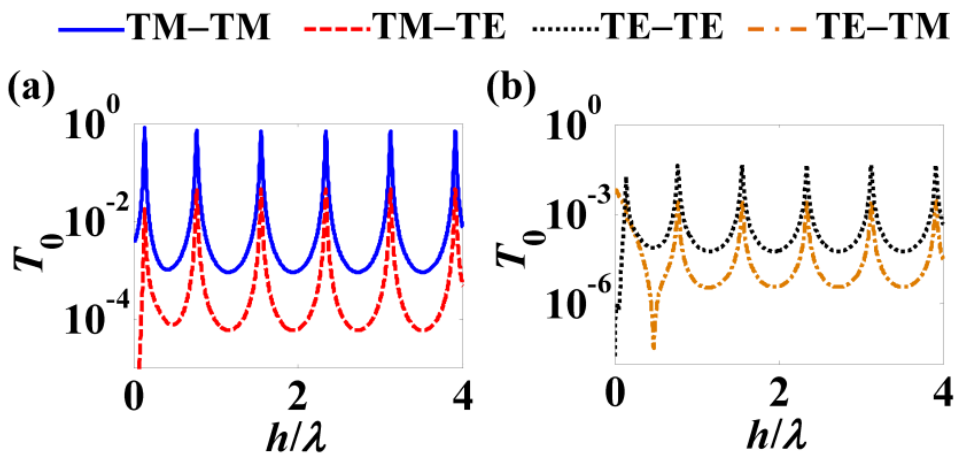

Figure S1. Transmission efficiency plotted as functions of the height *h* of the metamaterial cylinder, with the incident plane wave being TM polarized (a) and TE polarized (b). It can be identified that the transmission efficiency of TM-TE, TE-TE and TE-TM are much smaller than that of TM-TM.

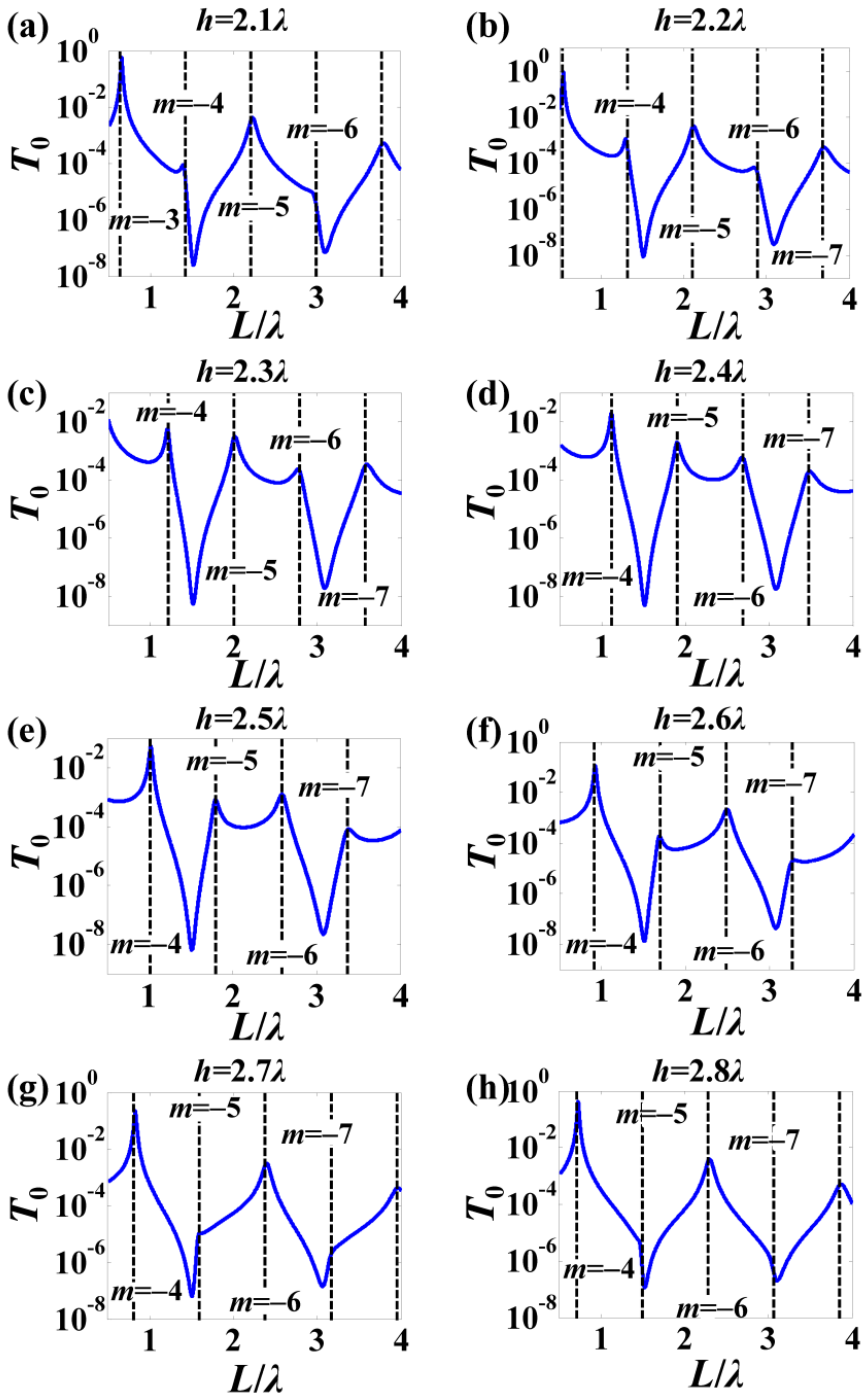

Figure S2. Transmission efficiency plotted as a function of the width of the metamaterial L calculated with Eq. (3) in the main text. (a)-(h) are for metamaterial height h=2.1λ, 2.2λ, 2.3λ, …, 2.8λ, respectively. The width L_{val} at the valley of the transmission efficiency is independent of the height h.

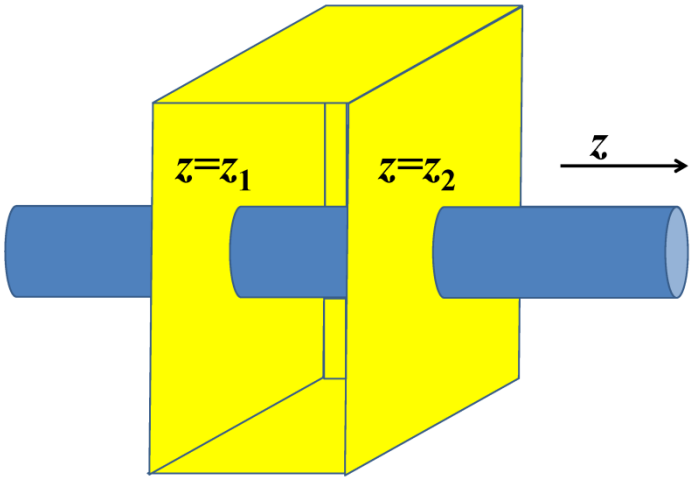

Figure S3. Sketch of reciprocal bi-anisotropic-medium waveguide, and waveguide modes are propagative in *z* direction. The yellow block represents the closed surface of the integration area in Eq. (S5).

Mode orthogonality in reciprocal bi-anisotropic-medium waveguide

We consider the waveguide as depicted in Fig. S3, the waveguide mode can be obtained by solving the source free Maxwell's Equations in frequency domain [1],

$$\nabla \times \mathbf{E} = -i\omega \mathbf{B}, \tag{S1a}$$

$$\nabla \times \mathbf{H} = i\omega \mathbf{D}, \tag{S1b}$$

where the magnetic induction **B** and electric displacement **D** satisfy the constitutive equation,

$$\mathbf{D} = \boldsymbol{\varepsilon}\mathbf{E} + i\boldsymbol{\gamma}\mathbf{H}, \tag{S2a}$$

$$\mathbf{B} = \boldsymbol{\mu}\mathbf{H} - i\boldsymbol{\gamma}\mathbf{E}, \tag{S2b}$$

If we use $\boldsymbol{\Phi}_1 = [\mathbf{E}_1, \mathbf{H}_1]$ and $\boldsymbol{\Phi}_2 = [\mathbf{E}_2, \mathbf{H}_2]$ to denote two waveguide modes with frequency ω_1 and ω_2, a set of differential equations can be derived

$$\nabla \times \mathbf{E}_1 = -i\omega_1 \boldsymbol{\mu}\mathbf{H}_1 - \omega_1 \boldsymbol{\gamma}\mathbf{E}_1, \nabla \times \mathbf{H}_1 = i\omega_1 \boldsymbol{\varepsilon}\mathbf{E}_1 - \omega_1 \boldsymbol{\gamma}\mathbf{H}_1, \tag{S3a}$$

$$\nabla \times \mathbf{E}_2 = -i\omega_2 \boldsymbol{\mu}\mathbf{H}_2 - \omega_2 \boldsymbol{\gamma}\mathbf{E}_2, \nabla \times \mathbf{H}_2 = i\omega_2 \boldsymbol{\varepsilon}\mathbf{E}_2 - \omega_2 \boldsymbol{\gamma}\mathbf{H}_2, \tag{S3b}$$

It can be easily deduced that

$$\begin{aligned} &\nabla\ (\mathbf{E}_2 \times \mathbf{H}_1) = (\nabla \times \mathbf{E}_2)\ \mathbf{H}_1 - \mathbf{E}_2\ (\nabla \times \mathbf{H}_1) \\ &= (-i\omega_2 \boldsymbol{\mu}\mathbf{H}_2 - \omega_2 \boldsymbol{\gamma}\mathbf{E}_2)\ \mathbf{H}_1 - \mathbf{E}_2\ (i\omega_1 \boldsymbol{\varepsilon}\mathbf{E}_1 - \omega_1 \boldsymbol{\gamma}\mathbf{H}_1) \end{aligned}, \tag{S4a}$$

$$\begin{aligned} &\nabla\ (\mathbf{E}_1 \times \mathbf{H}_2) = (\nabla \times \mathbf{E}_1)\ \mathbf{H}_2 - \mathbf{E}_1\ (\nabla \times \mathbf{H}_2) \\ &= (-i\omega_1 \boldsymbol{\mu}\mathbf{H}_1 - \omega_1 \boldsymbol{\gamma}\mathbf{E}_1)\ \mathbf{H}_2 - \mathbf{E}_1\ (i\omega_2 \boldsymbol{\varepsilon}\mathbf{E}_2 - \omega_2 \boldsymbol{\gamma}\mathbf{H}_2) \end{aligned}. \tag{S4b}$$

With the Gauss Ostrogradsky theorem, we obtain

$$\begin{aligned} &\iint_S (\mathbf{E}_2 \times \mathbf{H}_1 - \mathbf{E}_1 \times \mathbf{H}_2)\ d\mathbf{S} \\ &= \iiint_V [i(\omega_1 \mathbf{H}_2^{\mathrm{T}} \boldsymbol{\mu}\mathbf{H}_1 - \omega_2 \mathbf{H}_1^{\mathrm{T}} \boldsymbol{\mu}\mathbf{H}_2) + i(\omega_2 \mathbf{E}_1^{\mathrm{T}} \boldsymbol{\varepsilon}\mathbf{E}_2 - \omega_1 \mathbf{E}_2^{\mathrm{T}} \boldsymbol{\varepsilon}\mathbf{E}_1), \\ &\quad + (\omega_1 \mathbf{E}_2^{\mathrm{T}} \boldsymbol{\gamma}\mathbf{H}_1 - \omega_2 \mathbf{H}_1^{\mathrm{T}} \boldsymbol{\gamma}\mathbf{E}_2) + (\omega_1 \mathbf{H}_2^{\mathrm{T}} \boldsymbol{\gamma}\mathbf{E}_1 - \omega_2 \mathbf{E}_1^{\mathrm{T}} \boldsymbol{\gamma}\mathbf{H}_2)]dV \end{aligned} \tag{S5}$$

where S is a closed surface encompassing the volume V. The closed surface for the integration of Eq. (5) can be selected as the yellow block in Fig. S3. The two surfaces that are perpendicular to the z-axis extend to infinity in the transverse direction so that the

electromagnetic field of the bounded mode on the other surfaces of the block is zero. Thus the left side of Eq. (S5) can be simplified as

$$\iint_S (\mathbf{E}_2 \times \mathbf{H}_1 - \mathbf{E}_1 \times \mathbf{H}_2)\, d\mathbf{S} = \iint_{z_2} (\mathbf{E}_2 \times \mathbf{H}_1 - \mathbf{E}_1 \times \mathbf{H}_2)\, \mathbf{z} dS - \iint_{z_1} (\mathbf{E}_2 \times \mathbf{H}_1 - \mathbf{E}_1 \times \mathbf{H}_2)\, \mathbf{z} dS, \quad \text{(S6)}$$

The electromagnetic field in z_1 and z_2 planes has the relation $\mathbf{\Phi}_{1,z_2} = \exp(iq_1 D)\mathbf{\Phi}_{1,z_1}$, $\mathbf{\Phi}_{2,z_2} = \exp(iq_2 D)\mathbf{\Phi}_{2,z_1}$ (with q_1 and q_2 being the propagation constant), and thus we have

$$\begin{aligned} &\{1 - \exp[-i(q_1 + q_2)D]\} \iint_{z_2} (\mathbf{E}_2 \times \mathbf{H}_1 - \mathbf{E}_1 \times \mathbf{H}_2)\, \mathbf{z} dS \\ &= \iiint_V [i(\omega_1 \mathbf{H}_2^{\mathrm{T}} \boldsymbol{\mu} \mathbf{H}_1 - \omega_2 \mathbf{H}_1^{\mathrm{T}} \boldsymbol{\mu} \mathbf{H}_2) + i(\omega_2 \mathbf{E}_1^{\mathrm{T}} \boldsymbol{\varepsilon} \mathbf{E}_2 - \omega_1 \mathbf{E}_2^{\mathrm{T}} \boldsymbol{\varepsilon} \mathbf{E}_1) \\ &\quad + (\omega_1 \mathbf{E}_2^{\mathrm{T}} \boldsymbol{\gamma} \mathbf{H}_1 - \omega_2 \mathbf{H}_1^{\mathrm{T}} \boldsymbol{\gamma} \mathbf{E}_2) + (\omega_1 \mathbf{H}_2^{\mathrm{T}} \boldsymbol{\gamma} \mathbf{E}_1 - \omega_2 \mathbf{E}_1^{\mathrm{T}} \boldsymbol{\gamma} \mathbf{H}_2)] dV \end{aligned} \quad \text{(S7)}$$

Now we only consider the case of $\omega_1=\omega_2$. For reciprocal medium, there exist $\boldsymbol{\varepsilon}^{\mathrm{T}}=\boldsymbol{\varepsilon}$, $\boldsymbol{\mu}^{\mathrm{T}}=\boldsymbol{\mu}$ and $\boldsymbol{\gamma}^{\mathrm{T}}=\boldsymbol{\gamma}$, meaning $\mathbf{H}_2^{\mathrm{T}} \boldsymbol{\mu} \mathbf{H}_1 = \mathbf{H}_1^{\mathrm{T}} \boldsymbol{\mu} \mathbf{H}_2$, $\mathbf{E}_1^{\mathrm{T}} \boldsymbol{\varepsilon} \mathbf{E}_2 = \mathbf{E}_2^{\mathrm{T}} \boldsymbol{\varepsilon} \mathbf{E}_1$, $\mathbf{E}_2^{\mathrm{T}} \boldsymbol{\gamma} \mathbf{H}_1 = \mathbf{H}_1^{\mathrm{T}} \boldsymbol{\gamma} \mathbf{E}_2$, $\mathbf{H}_2^{\mathrm{T}} \boldsymbol{\gamma} \mathbf{E}_1 = \mathbf{E}_1^{\mathrm{T}} \boldsymbol{\gamma} \mathbf{H}_2$, and thus the right side of Eq. (S7) is zero. On the left side, if $\mathbf{\Phi}_1$ and $\mathbf{\Phi}_2$ are two different modes with the propagation constant $q_1 \neq -q_2$, the factor $1 - \exp[-i(q_1 + q_2)D] \neq 0$ and thus the surface integration $\iint_{z_2} (\mathbf{E}_2 \times \mathbf{H}_1 - \mathbf{E}_1 \times \mathbf{H}_2)\, \mathbf{z} dS = 0$. In contrast, if the two modes are the same mode and are counter propagative, we have $\iint_{z_2} (\mathbf{E}_2 \times \mathbf{H}_1 - \mathbf{E}_1 \times \mathbf{H}_2)\, \mathbf{z} dS \neq 0$. The mode orthogonality of the waveguide modes for reciprocal bi-anisotropic-medium waveguide can be demonstrated. The above derivation details are for bounded modes, for leaky modes, perfectly matched layers should be introduced to treat the divergence of the field at infinity. Detailed application of mode orthogonality of leaky modes is shown in Ref. [2].

References:

[1] Snyder, A. W., & Love, J. (2012). Optical waveguide theory. Springer Science & Business Media.

[2] Jia, H., Xie, Y., Liu, H., & Zhong, Y. (2016). Analytical model for the excitation of leaky surface plasmon polaritons in the attenuated total reflection configuration. Journal of Optics, 18(5), 055003.